ACS APPLIED MATERIALS & INTERFACES

Research Article

www.acsami.org

Scalable Hydrothermal Synthesis of Free-Standing VO_2 Nanowires in the M1 Phase

Gregory A. Horrocks,[†] Sujay Singh,[‡] Maliek F. Likely,[§] G. Sambandamurthy,[‡] and Sarbajit Banerjee*[,†]

[†]Department of Chemistry, Texas A&M University, College Station, Texas 77842-3012, United States

[‡]Department of Physics and [§]Department of Chemistry, University at Buffalo, The State University of New York, Buffalo, New York 14260, United States

ABSTRACT: VO_2 nanostructures derived from solution-phase methods are often plagued by broadened and relatively diminished metal−insulator transitions and adventitious doping due to imperfect control of stoichiometry. Here, we demonstrate a stepwise scalable hydrothermal and annealing route for obtaining VO_2 nanowires exhibiting almost 4 orders of magnitude abrupt (within 1 °C) metal−insulator transitions. The prepared nanowires have been characterized across their structural and electronic phase transitions using single-nanowire Raman microprobe analysis, ensemble differential scanning calorimetry, and single-nanowire electrical transport measurements. The electrical band gap is determined to be 600 meV and is consistent with the optical band gap of VO_2, and the narrowness of differential scanning calorimetry profiles indicates homogeneity of stoichiometry. The preparation of high-quality free-standing nanowires exhibiting pronounced metal−insulator transitions by a solution-phase process allows for scalability, further solution-phase processing, incorporation within nanocomposites, and integration onto arbitrary substrates.

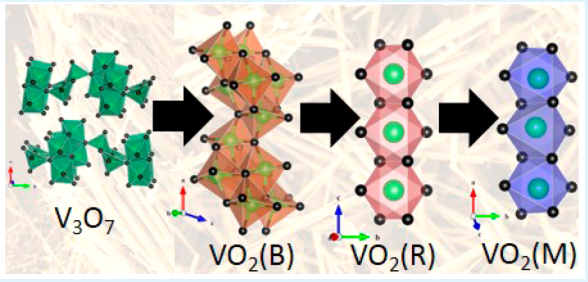

KEYWORDS: *devices, hydrothermal synthesis, metal−insulator transitions, nanowires, Raman spectroscopy, vanadium oxide*

INTRODUCTION

Vanadium(IV) dioxide, VO_2, has attracted significant research interest owing to its orders-of-magnitude first-order phase transition between insulating and metallic states that occurs at ca. 67 °C in the bulk.[1−3] The transition temperature, T_{MIT}, is uncommonly close to room temperature, and this fortunate circumstance has inspired considerable interest in device architectures that can take advantage of the abrupt switching of electrical and optical properties accompanying this phase transition.[1,2] A partial list of proposed device architectures that have been experimentally realized (to varying extents) includes Mott field transistors,[2,4] spectrally selective thermochromic glazings for "smart window" applications,[5] frequency-agile metamaterials for electromagnetic cloaking,[6] periodic oscillators,[7] memory devices based on two-terminal device configurations (mimicking neuromorphic circuits),[8,9] and strain sensors.[10−12] In addition, VO_2 has long served as an accessible system for fundamental explorations of strongly correlated behavior in materials.[1−3,13] The occurrence of a structural phase transformation between monoclinic and tetragonal phases in close proximity to the electronic transition temperature has led to contrasting views regarding the relative importance of electron−electron and electron−phonon interactions in VO_2.[1,14] However, it must be noted that the electronic and structural phase transitions can be separated for both thermally induced and photoactivated processes[15−17] in this system. Scaling VO_2 to finite sizes allows for more robust accommodation of the strain generated during the structural phase transformation (in other words, it enables protracted thermal cycling without cracking) and additionally allows for modification of the phase diagram to suppress the transition temperature and stabilize metastable phases.[12,18−20]

From a synthetic perspective, VO_2 is a challenging target since it is only stable within a narrow sliver of the V−O binary phase diagram[21] where it resides in immediate proximity to oxygen-deficient Magneli and Wadsley type phases wherein extended defects such as crystallographic shear planes facilitate accommodation of periodic arrays of oxygen vacancies.[22] The magnitude of the metal−insulator transition (for both optical and electrical properties) and T_{MIT} thus vary sensitively as a function of oxygen stoichiometry in VO_2.[21,23−25] Optimal control of the stoichiometry of VO_2 and thereby materials exhibiting the most pronounced (above 3 orders of magnitude) phase transitions have been realized thus far primarily by physical vapor deposition methods such as high-temperature vapor−solid deposition,[2,26−28] molecular beam epitaxy,[29,30] pulsed laser deposition,[19] and sputtering.[5,23] In these methods, the structure can be dictated on the basis of epitaxial homology with an underlying lattice-matched substrate, whereas the stoichiometry can be precisely defined by tuning the background pressure, precursor concentrations, and annealing conditions. Such variables tend to be more difficult to control

Received: April 26, 2014
Accepted: August 25, 2014
Published: August 25, 2014

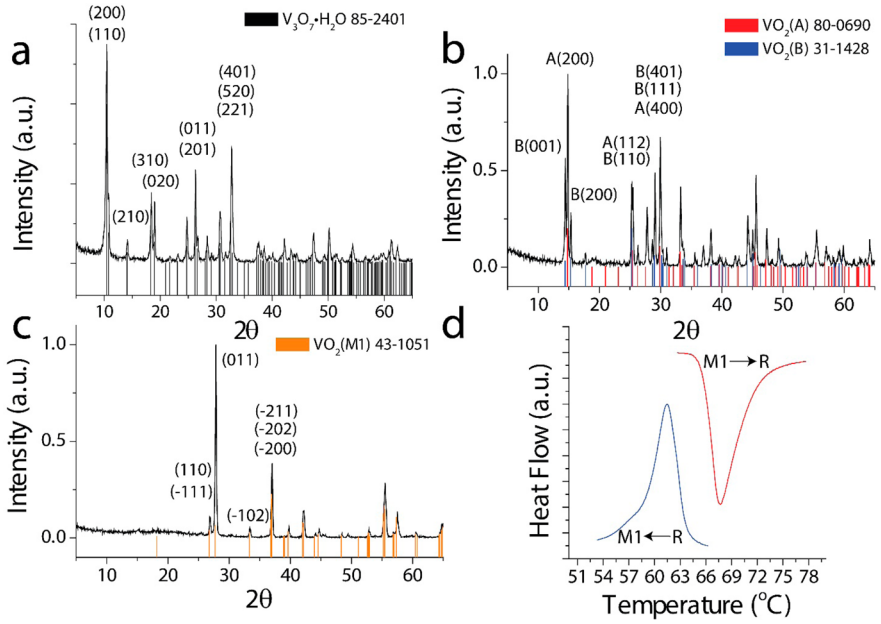

Figure 1. XRD patterns acquired for (a) as-synthesized $V_3O_7{\cdot}H_2O$ nanowires, (b) the initial mixture of VO_2 (A) and VO_2 (B) metastable phases obtained by reduction of $V_3O_7{\cdot}H_2O$ nanowires with a 1:1 (v/v) mixture of deionized water and 2-propanol, and (c) VO_2 nanowires after annealing at 475 °C for 1 h in an Ar ambient. (d) DSC plot of M1 VO_2 nanowires showing an exothermic transition upon heating centered at 67.5 °C and an endothermic transition upon cooling centered at 63.1 °C.

in solution-phase syntheses, and indeed, homogeneous nucleation tends to favor stabilization of a metastable VO_2(B) structure with the exception of reactions performed under high pressures.[31−33]

Solution-phase methods are desirable for improved scalability (applications such as deployment in thermochromic glazings and functional coatings will require much greater quantities of material than can possibly be obtained by physical vapor deposition) and cost-effectiveness and remain of paramount importance for obtaining high-quality materials that are decoupled from substrates. The last listed aspect is especially important for obtaining materials that can be cast onto arbitrary substrates as desired for a specific application, although modulation of the metal−insulator transition of VO_2 via lattice matching or substrate coupling also remains a rich area of study.[34] Obtaining free-standing nanowires further allows for deployment of surface functionalization and colloidal chemistry approaches, thereby enabling tuning of properties and incorporation within different matrixes and permitting the rational design of multicomponent nanocomposites. Sol−gel[35,36] and hydrothermal[33,37−39] approaches have previously been used to prepare VO_2 nanowires; the incorporation of W and Mo dopants appears to facilitate stabilization of the rutile (and, upon cooling to room temperature, the M1 monoclinic) phase of VO_2. However, examples of solution-based preparation of undoped VO_2 in nanoscale form are rare, and the materials thus prepared tend to be inferior to thin films and nanobeams obtained by vapor transport methods in terms of the magnitude of the switching evinced for the electrical conductivity and optical transmittance across the phase transition.[33,39−41]

In this work, we report a robust synthetic methodology that provides access to stoichiometry-controlled solution-derived VO_2 nanowires exhibiting massive metal−insulator transitions. Almost 4 orders of magnitude switching of resistance has been reproducibly realized for over 30 single-nanowire devices incorporating nanowires prepared by this method. For the prepared nanowires, both the structural and electronic phase transitions have been characterized. The availability of free-standing VO_2 nanowires allows for examination of the intrinsic phase diagram of the solution-derived nanostructures without obscuration from substrate coupling and strain imposed by mismatches in the coefficient of thermal expansion between the lattice and the substrate. Raman spectroscopy has been used to study the structural phase transformation given the drastically different Raman signatures of the two phases. The electronic phase transition in these nanowires has further been examined by individual nanowire electronic transport measurements after integration of the nanowires within device architectures.

EXPERIMENTAL SECTION

VO_2 nanowires were prepared by a stepwise hydrothermal method. First, nanowires of $V_3O_7{\cdot}H_2O$ were prepared via the hydrothermal exfoliation and reduction of bulk V_2O_5 (Sigma-Aldrich, 98%) by oxalic acid dihydrate (J.T. Baker). In a typical reaction, 300 mg of V_2O_5 was placed in a 23 mL PTFE cup with 16 mL of deionized water (ρ = 18.2 MΩ/cm, Barnstead International Nanopure Diamond) and 75 mg of oxalic acid dihydrate. The cup was then placed in a sealed autoclave and heated at a temperature of 210 °C for 72 h. This reaction can be reproducibly scaled using a 125 mL autoclave. For the large-scale reactions, 1.6304 g of V_2O_5 powder and 451 mg of oxalic acid dihydrate were reacted hydrothermally in 75 mL of deionized water. The resulting nanowires were filtered and washed with copious amounts of water and acetone.

The isolated $V_3O_7{\cdot}H_2O$ nanowires were then subsequently hydrothermally reduced by a 1:1 (v/v) mixture of water and 2-propanol (Fisher). In a typical reaction, 300 mg of the $V_3O_7{\cdot}H_2O$ nanowires were placed in a PTFE cup with 8 mL of deionized water and 8 mL of 2-propanol. The PTFE cup was then placed within a sealed autoclave and heated at a temperature of 210 °C for 72 h. The obtained mixture of VO_2(A) and VO_2(B) nanowires was isolated by filtration and washed with copious amounts of deionized water and acetone. Both hydrothermal reactions are performed at pressures of less than 125 bar, enabling the use of low-pressure autoclaves. The collected nanowires (mixture of VO_2(A) and VO_2(B)) were

subsequently annealed at 475 °C under an Ar atmosphere in a tube furnace while an Ar flow of 150 mL/min was maintained for 1 h; VO_2 nanowires crystallized in the M1 phase were recovered after cooling to room temperature.

Powder X-ray diffraction (XRD) characterization of the prepared materials was performed using a Rigaku Ultima IV diffractometer (Cu Kα radiation, voltage of 40 kV, current of 44 mA). JADE 8.5 was used for pattern fitting and phase identification. Differential scanning calorimetry (DSC; Q200 TA Instruments) was performed between −50 and +150 °C under a flowing Ar atmosphere. The morphology and purity of the obtained nanowires were examined by scanning electron microscopy coupled with energy-dispersive X-ray spectoscopy (SEM−EDX; Hitachi SU-70 operated at 15 kV) and transmission electron microscopy (TEM; JEOL JEM-2010 operated at an accelerating voltage of 200 kV). TEM samples were prepared by dispersing nanowires in 2-propanol by ultrasonication, and casting onto 400 mesh copper grids coated with a Formvar/carbon film.

Raman spectra were acquired using a Jobin-Yvon Horiba Labram HR instrument coupled to an Olympus BX41 microscope. The 514.5 nm line from an Ar ion laser was used as the excitation source. The Raman spectra were acquired using a 1800 lines/mm grating, yielding a spectral resolution of better than 2 cm^{-1}. The in situ heating measurements were performed under a N_2 atmosphere using a sealed THMS 600 thermal stage from Linkam Scientific Instruments. The samples were left to equilibrate at each temperature for 300 s prior to the Raman spectrum being acquired.

Electrical transport measurements of single nanowires were performed using a variable-temperature cryostat insert. The nanowires were first dispersed and cast onto Si/SiO_2 (300 nm) substrates. Subsequently, Au electrodes (70 nm) were patterned after contacts to the nanowires were defined using a combination of electron-beam lithography and photolithography; Cr metal (5 nm) was used as the adhesion layer. Resistance versus temperature measurements were acquired for both heating and cooling cycles between 27 and 107 °C. Current versus voltage measurements were acquired using single-nanowire devices fabricated by the same method. The current across the devices was measured by sweeping the voltage between 0 and 2 V while holding the temperature constant.

RESULTS AND DISCUSSION

The prepared nanomaterials have been characterized across the successive reductive steps as well as across the structural and electronic phase transitions of VO_2. Figure 1 illustrates the characterization of the nanowires through each step of the synthetic approach. The hydrothermal reduction of V_2O_5 by oxalic acid yields phase-pure $V_3O_7{\cdot}H_2O$ nanowires as per the following reaction:

$$3V_2O_5(s) + H_2C_2O_4(aq) \xrightarrow{\text{hydrothermal}} 2V_3O_7{\cdot}H_2O(s) + 2CO_2(g) \quad (1)$$

Figure 1a indicates the XRD pattern acquired for these nanowires, which can be indexed to PDF No. 84-2801. Parts a and b of Figure 2 show SEM and TEM images of $V_3O_7{\cdot}H_2O$ nanowires. The nanowires are 183 ± 34 nm wide and range up to hundreds of micrometers in length. The subsequent hydrothermal reduction of V_3O_7 using a mixture of 2-propanol and water as per

$$V_3O_7{\cdot}H_2O(s) + 2(CH_3)_2CHOH \xrightarrow{\text{hydrothermal}} 3VO_2(s) + 2(CH_3)_2CHO(aq) + 2H_2O(l) \quad (2)$$

yields a mixture of the metastable VO_2(A) (PDF No. 80-0690) and VO_2(B) (PDF No. 31-1428) phases as illustrated by the XRD pattern shown in Figure 1b. Oxalic acid and citric acid can also be used for the reduction of $V_3O_7{\cdot}H_2O$ and do yield a similar mix of VO_2(A) and VO_2(B) phases; however, the obtained materials are poorly defined in terms of their morphologies. 2-Propanol appears to be the optimal reducing/structure-directing agent for obtaining well-defined nanowires. Reaction using just deionized water yields the metastable VO_2(B) phase but with a substantial amount of other mixed-valence vanadium oxide phases resulting from incomplete reduction. While reaction with other small aliphatic molecules

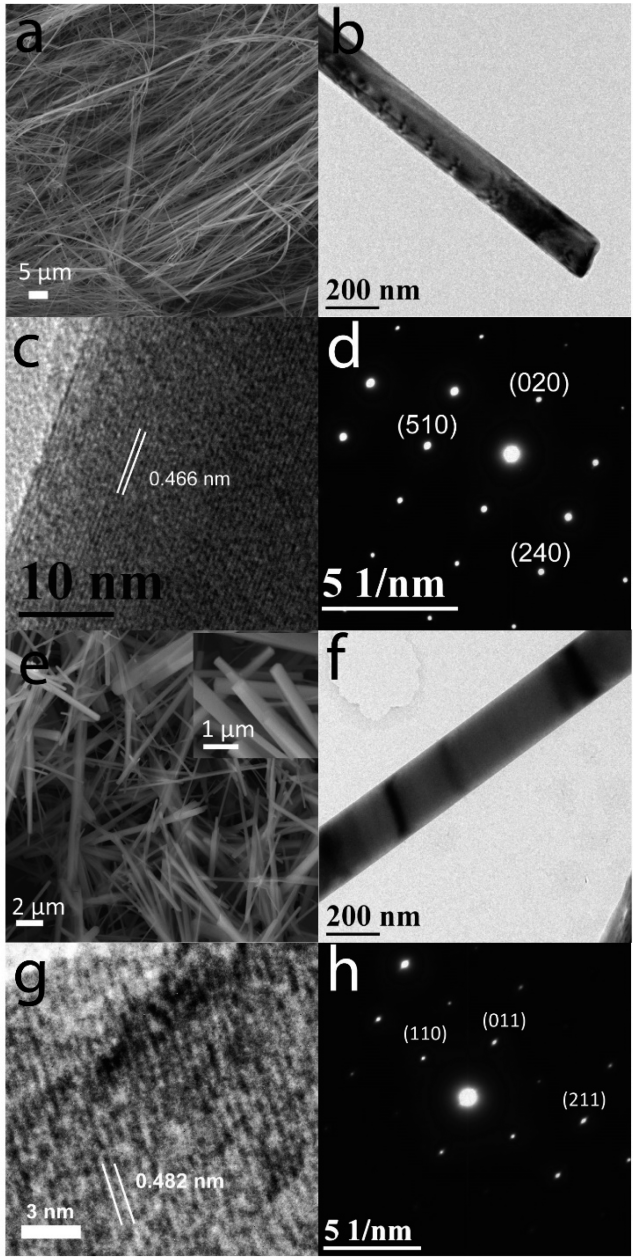

Figure 2. (a) SEM and (b) TEM images of $V_3O_7{\cdot}H_2O$ nanowires. (c) Lattice-resolved HRTEM image of $V_3O_7{\cdot}H_2O$ nanowires indicating an interplanar separation of 0.466 nm corresponding to the spacing between (020) lattice planes. (d) Indexed SAED pattern acquired for an individual $V_3O_7{\cdot}H_2O$ nanowire. (e) SEM image of monoclinic VO_2 nanowires with the inset indicating rectangular cross sections. (f) TEM image of a monoclinic VO_2 nanowire. (g) HRTEM image of a monoclinic M1 phase VO_2 nanowire indicating an interplanar separation of 0.482 nm. (h) Indexed SAED pattern acquired for an individual monoclinic VO_2 nanowire.

yields similar mixtures of the two metastable phases after reduction, the overall particle size remains significantly larger than that achieved via the 2-propanol reduction. Upon annealing the products of the 2-propanol reduction reaction, the M1 phase of VO_2 is recovered as illustrated in Figure 1c. At temperatures of less than 450 °C, there is evidence for substantial remnant VO_2(B). The VO_2(A) and VO_2(B) phases have less close packed frameworks with greater void space and have been predicted to undergo an order−disorder transition with eventual recrystallization into the rutile phase of VO_2, which subsequently transforms to the M1 monoclinic phase upon cooling.[31] Fortuitously, for loosely packed powders of VO_2 nanowires, the transformation is induced well before initiation of sintering, allowing for retention of the morphology originally defined by the hydrated V_3O_7 nanowires. Conversely, annealing under an air or oxygen ambient under the same conditions yields phase-pure V_2O_5 nanowires without appreciable sintering and with similar dimensions.[42] Note that the annealing step is performed on the powder samples and the resulting nanowires synthesized on the multigram scale are available for incorporation onto arbitrary substrates or within host matrices including polymers.

The thermally and electrically induced M1 → R phase transition is first order in nature and accompanied by a substantial change in thermal conductivity as well as a discontinuous jump in carrier concentration. Being a first-order phase transition, the structural phase transformation is associated with a substantial latent heat and alteration of the specific heat capacity.[43,44] The latent heat at the phase transition arises from the structural distortion of the lattice and the change in entropy of the conduction electrons (which are no longer localized in the insulating state).[40,43] Figure 1d shows pronounced endothermic and exothermic DSC profiles for the VO_2 nanowires centered at 67.5 and 61.3 °C upon heating and cooling, respectively. The fwhm values of the DSC profiles are 3.8 and 3.0 °C, respectively. These fwhm values are much narrower than the 10−15 °C fwhm values observed previously for solution-derived undoped and W-doped VO_2 nanowires.[37] As an ensemble measurement across multiple nanowires, the width of the observed transition reflects the distribution of temperatures at which the nanowires are undergoing the metal−insulator transition. The narrower ensemble DSC profile implies greater homogeneity of the transition temperature across the nanowire sample, indicating much tighter stoichiometric control of the prepared nanowires. The latent heat of the endothermic insulator → metal transition is determined to be 7.88 J/g on the basis of integration of the area of the transition.

Figure 2e depicts SEM images of the monoclinic VO_2 nanowires after annealing and shows well-defined nanowires with rectangular cross sections and lengths on the order of tens of micrometers, while EDX analysis indicates no inadvertent dopant inclusion during the synthetic procedure. TEM images of the nanowires indicate an average width of 187 ± 77 nm (Figure 2f), essentially retaining the lateral dimensions of the original $V_3O_7{\cdot}H_2O$ precursor nanowires with some fragmentation resulting from the order−disorder transition discussed above. Lattice-resolved HRTEM images (Figure 2g) and the selected area electron diffraction (SAED) patterns acquired for an individual nanowire (Figure 2h) corroborate the phase assignment to the M1 monoclinic phase of VO_2. The lattice-resolved HRTEM image in Figure 2g indicates an interplanar separation of 0.481 nm, which corresponds to the separation between the (100) planes of monoclinic VO_2.

Raman microprobe analysis provides an excellent spatially localized probe of the structural progression of the phase transition in VO_2.[45−48] The M1 monoclinic, M2 monoclinic, triclinic, and rutile phases of VO_2 have distinctive Raman spectral signatures arising from their varying local symmetry. The rutile and M1 phases crystallize in $P4_2/mnm$ (D_{4h}^{14}) and $P2_1/c$ (C_{2h}^{3}) space groups, respectively, with the latter predicted to have 18 Raman-allowed modes, 9 each of A_g and B_g symmetry.[48,49] Raman spectra have been acquired for individual VO_2 nanowires (by dispersing the nanowires shown in Figure 2e on a glass substrate) as a function of temperature across the metal−insulator transition. The spectra for a representative nanowire are depicted in Figure 3. The modes

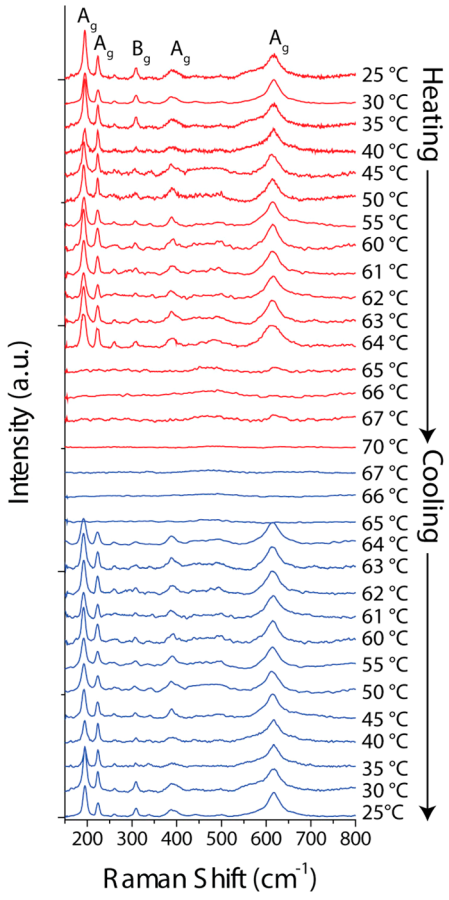

Figure 3. Raman spectra acquired for an individual VO_2 nanowire upon heating and cooling across the metal−insulator transition. Upon heating, all Raman-active modes of the insulating M1 monoclinic phase are lost when the nanowire transitions to the high-symmetry metallic rutile phase between 64 and 65 °C. The nanowire then transitions back to the M1 phase upon cooling between 65 and 64 °C.

observed at low temperatures can be assigned to the M1 monoclinic phase of VO_2, with the symmetry assignments denoted in the figure derived from group theory considerations and previously published polarized Raman spectroscopy studies.[48−50] In contrast, the rutile phase has a much lower Raman cross section and does not exhibit distinct modes in keeping with its metallic character (the laser skin depth is also greatly diminished by the much greater concentration of carriers in the metallic phase). Upon heating the VO_2 nanowire

under a nitrogen ambient, the Raman spectrum does not show much of a change until between 64 and 65 °C an abrupt and sudden loss of all Raman-active modes is evidenced, indicating complete conversion to the metallic rutile phase. Remarkably, the transition is not preceded by any discernible attenuation of intensity or shifts of the Raman modes, suggesting that the entire nanowire is transformed as a single domain (within the limits of experimental resolution). The Raman modes are further recovered upon cooling back to 64 °C.

Unlike VO_2 nanobeams coupled to substrates grown by vapor transport, there is no evidence in the Raman data for stabilization of the M2 phase (which crystallizes in the C_{2h}^5 space group and is characterized by a splitting of the A_g mode at 221 cm^{-1} and a shift of the A_g mode at 607 cm^{-1} to 649 cm^{-1}). Consistent with the narrow line shapes of the ensemble DSC profiles, the sharp discontinuities noted here are surmised to result from improved homogeneity in stoichiometry across the nanowires.

The pronounced switching behavior thought to be characteristic of stoichiometric VO_2 is most patently manifested in electrical transport measurements of individual nanowires across their metal−insulator transitions induced by temperature or voltage, as depicted in Figure 4. Note that the nanowires have been solution cast (from 2-propanol dispersions) onto Si/SiO_2 (300 nm) substrates and no effort has been invested in liberating the nanowires from the substrate as was previously required to observe abrupt transitions for nanobeams deposited by vapor transport where coupling to the substrate induces inhomogeneous strain.[27,51] Figure 4a illustrates that the transition from the insulating to the metallic phase is characterized by a greater than 3 (almost 4) orders of magnitude decrease in resistance across a span of just 0.1 °C; the transition back to the insulating phase is similarly abrupt with the hysteresis of 13.2 °C derived from the first-order nature of the transition. The Arrhenius behavior in the insulating phase of the nanowires is well fitted with $R(T) = R_0 \exp(E_g/2kT)$ (where k is Boltzmann's constant and T is temperature) and yields an electrical band gap (E_g) of 600 meV, which is consistent with the values observed for suspended VO_2 nanobeams and indeed the optical band gap of VO_2.[51] The band gap for these nanowires is significantly greater than the 80−200 meV values observed previously for solution-grown W-doped VO_2 nanowires[41] and confirms the tight control of stoichiometry and the absence of inadvertent doping. Dimensional confinement in high-crystalline-quality nanostructures limits the number of possible nucleation sites and thereby can kinetically inhibit initiation of a phase transformation, yielding a greater hysteresis than observed in the bulk.[52] Of the 30 devices tested (each comprising an individual nanowire), the insulator → metal transition has been observed at a temperature of 71 ± 2 °C, with the transition spanning no greater than 1 °C. The abruptness of these transitions is in stark contrast to previous observations for hydrothermally prepared and especially doped nanostructures that typically show broader insulator → metal (or metal → insulator) profiles spanning 3−5 °C for undoped VO_2 and ranging up to 10−20 °C for doped samples.[18,38,51,53,54] The current versus voltage plots depicted in Figure 4b are analogously characterized by sharp switching of the conductivity above a threshold voltage, with the threshold voltage required to trigger the transition being inversely correlated to temperature. For temperatures below T_{MIT}, upon reaching the specific threshold voltage, a discontinuous increase in current is evidenced, indicating a transition to a metallic phase. In the insulator → metal direction, the threshold voltage (V_{th}) for the transition shows an approximately exponential $V_{th} \propto \exp(-T/T_0)$ dependence that is characteristic of a charge delocalization in a charge-ordered system.[40,55,56] In other words, the nonequilibrium application of an electric field injects carriers into the nanowires. Beyond a critical carrier density, Thomas−Fermi screening of bound excitonic states by the injected free carriers leads to an abrupt increase of the carrier density, resulting in transformation of the system to a metallic state even at low temperatures. At low temperatures, a sharp singular, almost step-function-like, jump is noted upon reaching the threshold voltage; at temperatures approaching (but less than) T_{MIT}, a number of discontinuous jumps are observed that are attributed to progression of the phase transition through avalanche-type events and the stabilization of a strongly correlated metallic phase.[57,58] Thermal effects are convoluted with the electric-field-induced effects closer to the transition temperature, whereas the electric-field-induced delocalization of charge-ordering motifs is more clearly observed at low temperatures.[58] Above T_{MIT}, no voltage-induced metal−insulator transition is evidenced, and instead, a linear current versus voltage trace is observed, indicating that the VO_2 nanowire is already in a metallic state. The abruptness of the metal−insulator transition evidenced in both the thermal and electric-field-induced transitions further corroborates the good

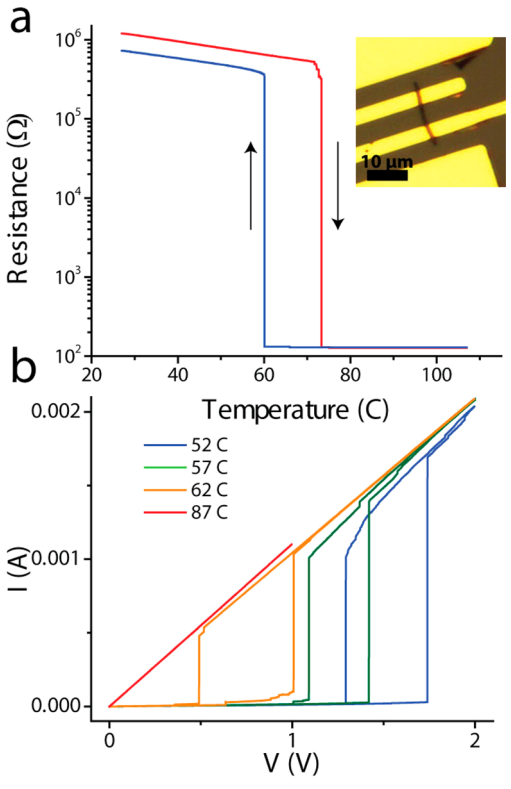

Figure 4. (a) Resistance versus temperature measured for an individual-nanowire device indicating a transition between the insulating and metallic phases within 0.1 °C at 73.3 °C. The inset depicts an optical micrograph of the device. (b) Current versus voltage measurements for single-nanowire devices show abrupt voltage-driven transitions between the insulating and metallic phases at temperatures below the transition temperature. The threshold voltage required to induce the insulator → metal transition is clearly decreased with increasing temperature.

crystalline quality and tight stoichiometric control of the VO_2 nanowires.

CONCLUSIONS

In conclusion, a novel stepwise hydrothermal methodology has been developed for preparing phase-pure VO_2 nanowires based on the initial oxalic acid reduction of V_2O_5 powders to $V_3O_7 \cdot H_2O$ nanowires that are subsequently reduced to a mixture of VO_2(A) and VO_2(B) nanowires with the help of 2-propanol. The latter metastable phases are converted to the rutile phase of VO_2 upon annealing, allowing for recovery of monoclinic M1 VO_2 nanowires with controlled stoichiometry upon cooling. The nanowires exhibit abruptly discontinuous phase transitions exceeding 3 (and approaching 4) orders of magnitude in electrical transport measurements, as well as sharp ensemble DSC profiles and dramatic changes of Raman spectra at the transition temperature, suggesting that this solution-phase methodology yields VO_2 nanowires of comparable quality and carefully controlled stoichiometry as derived from physical vapor transport methods. The electrical band gap for the synthesized nanowires is 600 meV, consistent with the optical band gap of VO_2, verifying the close control of stoichiometry. The process devised here is scalable and yields free-standing nanowires that can be dispersed on arbitrary substrates or incorporated within composite materials.

AUTHOR INFORMATION

Corresponding Author

*E-mail: banerjee@chem.tamu.edu. Phone: 979-862-3102.

Notes

The authors declare no competing financial interest.

ACKNOWLEDGMENTS

This work was primarily supported by the National Science Foundation under Grant IIP 1311837 as well as by Quanex Building Products. S.S. and S.G. acknowledge support from the National Science Foundation under Grant DMR 0847324.

REFERENCES

(1) Whittaker, L.; Patridge, C. J.; Banerjee, S. Microscopic and Nanoscale Perspective of the Metal-Insulator Phase of VO_2: Some New Twists to an Old Tale. *J. Phys. Chem. Lett.* **2011**, *2*, 745−758.

(2) Yang, Z.; Ko, C.; Ramanathan, S. Oxide Electronics Utilizing Ultrafast Metal-Insulator Transitions. *Annu. Rev. Mater. Res.* **2011**, *41*, 337−367.

(3) Imada, M.; Fujimori, A.; Tokura, Y. Metal-Insulator Transitions. *Rev. Mod. Phys.* **1998**, *70*, 1039−1263.

(4) Ruzmetov, D.; Gopalakrishnan, G.; Ko, C.; Narayanamurti, V.; Ramanathan, S. Three-Terminal Field Effect Devices Utilizing Thin Film Vanadium Oxide as the Channel Layer. *J. Appl. Phys.* **2010**, *107*, 114516.

(5) Li, S.-Y.; Namura, K.; Suzuki, M.; Niklasson, G. A.; Granqvist, C. G. Thermochromic VO_2 Nanorods Made by Sputter Deposition: Growth Conditions and Optical Modeling. *J. Appl. Phys.* **2013**, *114*, 033516.

(6) Driscoll, T.; Kim, H.-T.; Chae, B.-G.; Kim, B.-J.; Lee, Y.-W.; Jokerst, N. M.; Palit, S.; Smith, D. R.; Di Ventra, M.; Basov, D. N. Memory Metamaterials. *Science* **2009**, *325*, 1518−1521.

(7) Driscoll, T.; Quinn, J.; Di Ventra, M.; Basov, D. N.; Seo, G.; Lee, Y.-W.; Kim, H.-T.; Smith, D. R. Current Oscillations in Vanadium Dioxide: Evidence for Electrically Triggered Percolation Avalanches. *Phys. Rev. B* **2012**, *86*, 094203−1.

(8) Jo, S. H.; Chang, T.; Ebong, I.; Bhadviya, B. B.; Mazumder, P.; Lu, W. Nanoscale Memristor Device as Synapse in Neuromorphic Systems. *Nano Lett.* **2010**, *10*, 1297−1301.

(9) Strukov, D. B.; Snider, G. S.; Stewart, D. R.; Williams, R. S. The Missing Memristor Found. *Nature* **2008**, *453*, 80−83.

(10) Wu, C.; Feng, F.; Xie, Y. Design of Vanadium Oxide Structures with Controllable Electrical Properties for Energy Applications. *Chem. Soc. Rev.* **2013**, *42*, 5157−5183.

(11) Li, S.; Li, Y.; Jiang, M.; Ji, S.; Luo, H.; Gao, Y.; Jin, P. Preparation and Characterization of Self-Supporting Thermochromic Films Composed of VO_2(M)@SiO_2 Nanofibers. *ACS Appl. Mater. Interfaces* **2013**, *5*, 6453−6457.

(12) Cao, J.; Ertekin, E.; Srinivasan, V.; Fan, W.; Huang, S.; Zheng, H.; Yim, J. W. L.; Khanal, D. R.; Ogletree, D. F.; Grossman, J. C.; Wu, J. Strain Engineering and One-Dimensional Organization of Metal−Insulator Domains in Single-Crystal Vanadium Dioxide Beams. *Nat. Nanotechnol.* **2009**, *4*, 732−737.

(13) Yamauchi, T.; Ueda, Y. Superconducting $\beta(\beta')$-Vanadium Bronzes under Pressure. *Phys. Rev. B* **2008**, *77*, 1−18.

(14) Eyert, V. VO_2: A Novel View from Band Theory. *Phys. Rev. Lett.* **2011**, *107*, 016401.

(15) Qazilbash, M. M.; Tripathi, A.; Schafgans, A. A.; Kim, B.-J.; Kim, H.-T.; Cai, Z.; Holt, M. V.; Maser, J. M.; Keilmann, F.; Shpyrko, O. G.; Basov, D. N. Nanoscale Imaging of the Electronic and Structural Transitions in Vanadium Dioxide. *Phys. Rev. B* **2011**, *83*, 165108.

(16) Tao, Z.; Han, T.-R. T.; Mahanti, S. D.; Duxbury, P. M.; Yuan, F.; Ruan, C.-Y.; Wang, K.; Wu, J. Decoupling of Structural and Electronic Phase Transitions in VO_2. *Phys. Rev. Lett.* **2012**, *109*, 166406.

(17) Van Veenendaal, M. Ultrafast Photoinduced Insulator-to-Metal Transitions in Vanadium Dioxide. *Phys. Rev. B* **2013**, *87*, 235118.

(18) Cao, J.; Gu, Y.; Fan, W.; Chen, L. Q.; Ogletree, D. F.; Chen, K.; Tamura, N.; Kunz, M.; Barrett, C.; Seidel, J.; Wu, J. Extended Mapping and Exploration of the Vanadium Dioxide Stress-Temperature Phase Diagram. *Nano Lett.* **2010**, *10*, 2667−2673.

(19) Lopez, R.; Feldman, L.; Haglund, R. Size-Dependent Optical Properties of VO_2 Nanoparticle Arrays. *Phys. Rev. Lett.* **2004**, *93*, 177403.

(20) Lopez, R.; Boatner, L. A.; Haynes, T. E.; Feldman, L. C.; Haglund, R. F. Synthesis and Characterization of Size-Controlled Vanadium Dioxide Nanocrystals in a Fused Silica Matrix. *J. Appl. Phys.* **2002**, *92*, 4031.

(21) Griffiths, C. H. Influence of Stoichiometry on the Metal-Semiconductor Transition in Vanadium Dioxide. *J. Appl. Phys.* **1974**, *45*, 2201.

(22) Katzke, H.; Tolédano, P.; Depmeier, W. Theory of Morphotropic Transformations in Vanadium Oxides. *Phys. Rev. B* **2003**, *68*, 024109.

(23) Ruzmetov, D.; Zawilski, K. T.; Narayanamurti, V.; Ramanathan, S. Structure-Functional Property Relationships in Rf-Sputtered Vanadium Dioxide Thin Films. *J. Appl. Phys.* **2007**, *102*, 113715.

(24) Narayan, J.; Bhosle, V. M. Phase Transition and Critical Issues in Structure-Property Correlations of Vanadium Oxide. *J. Appl. Phys.* **2006**, *100*, 103524.

(25) Youn, D.-H.; Kim, H.-T.; Chae, B.-G.; Hwang, Y.-J.; Lee, J.-W.; Maeng, S.-L.; Kang, K.-Y. Phase and Structural Characterization of Vanadium Oxide Films Grown on Amorphous SiO_2/Si Substrates. *J. Vac. Sci. Technol., A* **2004**, *22*, 719.

(26) Guiton, B. S.; Gu, Q.; Prieto, A. L.; Gudiksen, M. S.; Park, H. Single-Crystalline Vanadium Dioxide Nanowires with Rectangular Cross Sections. *J. Am. Chem. Soc.* **2005**, *127*, 498−499.

(27) Wu, J.; Gu, Q.; Guiton, B. S.; Leon, N. P.; De Ouyang, L.; Park, H. Strain-Induced Self Organization of Metal−Insulator Domains in. *Nano Lett.* **2006**, *6*, 2313−2317.

(28) Manning, T. D.; Parkin, I. P.; Clark, R. J. H.; Sheel, D.; Pemble, M. E.; Vernadou, D. Intelligent Window Coatings: Atmospheric Pressure Chemical Vapour Deposition of Vanadium Oxides. *J. Mater. Chem.* **2002**, *12*, 2936−2939.

(29) Tashman, J. W.; Lee, J. H.; Paik, H.; Moyer, J. A.; Misra, R.; Mundy, J. A.; Spila, T.; Merz, T. A.; Schubert, J.; Muller, D. A.;

Schiffer, P.; Schlom, D. G. Epitaxial Growth of VO_2 by Periodic Annealing. *Appl. Phys. Lett.* **2014**, *104*, 063104.
(30) Fan, L. L.; Chen, S.; Wu, Y. F.; Chen, F. H.; Chu, W. S.; Chen, X.; Zou, C. W.; Wu, Z. Y. Growth and Phase Transition Characteristics of Pure M-Phase VO_2 Epitaxial Film Prepared by Oxide Molecular Beam Epitaxy. *Appl. Phys. Lett.* **2013**, *103*, 131914.
(31) Leroux, C.; Nihoul, G.; Van Tendeloo, G. From VO_2(B) to VO_2(R): Theoretical Structures of VO_2 Polymorphs and in Situ Electron Microscopy. *Phys. Rev. B* **1998**, *57*, 5111−5121.
(32) Oka, Y.; Sato, S.; Yao, T.; Yamamoto, N. Crystal Structures and Transition Mechanism of VO_2(A). *J. Solid State Chem.* **1998**, 594−598.
(33) Whittaker, L.; Zhang, H.; Banerjee, S. VO_2 Nanosheets Exhibiting a Well-Defined Metal−Insulator Phase Transition. *J. Mater. Chem.* **2009**, *19*, 2968.
(34) Liu, M.; Wagner, M.; Zhang, J.; McLeod, A.; Kittiwatanakul, S.; Fei, Z.; Abreu, E.; Goldflam, M.; Sternbach, A. J.; Dai, S.; West, K. G.; Lu, J.; Wolf, S. A.; Averitt, R. D.; Basov, D. N. Symmetry Breaking and Geometric Confinement in VO_2: Results from a Three-Dimensional Infrared Nano-Imaging. *Appl. Phys. Lett.* **2014**, *104*, 121905.
(35) Mai, L. Q.; Hu, B.; Hu, T.; Chen, W.; Gu, E. D. Electrical Property of Mo-Doped VO_2 Nanowire Array Film by Melting−Quenching Sol−Gel Method. *J. Phys. Chem. B* **2006**, *110*, 19083−19086.
(36) Pan, M.; Zhong, H.; Wang, S.; Liu, J.; Li, Z.; Chen, X.; Lu, W. Properties of VO_2 Thin Film Prepared with Precursor $VO(acac)_2$. *J. Cryst. Growth* **2004**, *265*, 121−126.
(37) Whittaker, L.; Jaye, C.; Fu, Z.; Fischer, D. A.; Banerjee, S. Depressed Phase Transition in Solution-Grown VO_2 Nanostructures. *J. Am. Chem. Soc.* **2009**, *131*, 8884−8894.
(38) Corr, S. A.; Grossman, M.; Furman, J. D.; Melot, B. C.; Cheetham, A. K.; Heier, K. R.; Seshadri, R. Controlled Reduction of Vanadium Oxide Nanoscrolls: Crystal Structure, Morphology, and Electrical Properties. *Chem. Mater.* **2008**, *20*, 6396−6404.
(39) Liu, J.; Li, Q.; Wang, T.; Yu, D.; Li, Y. Metastable Vanadium Dioxide Nanobelts: Hydrothermal Synthesis, Electrical Transport, and Magnetic Properties. *Angew. Chem., Int. Ed.* **2004**, *43*, 5048−5052.
(40) Whittaker, L.; Wu, T.-L.; Patridge, C. J.; Sambandamurthy, G.; Banerjee, S. Distinctive Finite Size Effects on the Phase Diagram and Metal−Insulator Transitions of Tungsten-Doped Vanadium(IV) Oxide. *J. Mater. Chem.* **2011**, *21*, 5580.
(41) Wu, T.; Whittaker, L.; Banerjee, S.; Sambandamurthy, G. Temperature and Voltage Driven Tunable Metal-Insulator Transition in Individual $W_xV_{1-x}O_2$ Nanowires. *Phys. Rev. B* **2011**, *83*, 073101.
(42) Horrocks, G. A.; Likely, M. F.; Velazquez, J. M.; Banerjee, S. Finite Size Effects on the Structural Progression Induced by Lithiation of V_2O_5: A Combined Diffraction and Raman Spectroscopy Study. *J. Mater. Chem. A* **2013**, *1*, 15265.
(43) Berglund, C. N.; Guggenheim, H. J. Electronic Properties of VO_2 near the Semiconductor-Metal Transition. *Phys. Rev.* **1969**, *185*, 1022−1033.
(44) Salker, A. V.; Seshan, K.; Keer, H. V. Phase Transition Behaviour of VO_2. *Phys. Status Solidi A* **1983**, *75*, K37−K40.
(45) Whittaker, L.; Wu, T.; Stabile, A.; Sambandamurthy, G.; Banerjee, S. Single-Nanowire Raman Microprobe Studies of Doping-, Temperature-, and Voltage-Induced Metal−Insulator Transitions of $W_xV_{1-x}O_2$ Nanowires. *ACS Nano* **2011**, *5*, 8861−8867.
(46) Zhang, S.; Chou, J. Y.; Lauhon, L. J. Direct Correlation of Structural Domain Formation with the Metal Insulator Transition in a VO_2 Nanobeam. *Nano Lett.* **2009**, *9*, 4527−4532.
(47) Donev, E. U.; Lopez, R.; Feldman, L. C.; Haglund, R. F. Confocal Raman Microscopy across the Metal−Insulator Transition of Single Vanadium Dioxide Nanoparticles. *Nano Lett.* **2009**, *9*, 702−706.
(48) Jones, A. C.; Berweger, S.; Wei, J.; Cobden, D.; Raschke, M. B. Nano-Optical Investigations of the Metal−Insulator Phase Behavior of Individual VO_2 Microcrystals. *Nano Lett.* **2010**, *10*, 1574−1581.
(49) Schilbe, P. Raman Scattering in VO_2. *Physica B* **2002**, *316-317*, 600−602.
(50) Chou, J. Y.; Lensch-Falk, J. L.; Hemesath, E. R.; Lauhon, L. J. Vanadium Oxide Nanowire Phase and Orientation Analyzed by Raman Spectroscopy. *J. Appl. Phys.* **2009**, *105*, 034310.
(51) Wei, J.; Wang, Z.; Chen, W.; Cobden, D. H. New Aspects of the Metal−Insulator Transition in Single-Domain Vanadium Dioxide Nanobeams. *Nat. Nanotechnol* **2009**, *4*, 420.
(52) Waitz, T.; Tsuchiya, K.; Antretter, T.; Fischer, F. D. Phase Transformations of Nanocrystalline Martensitic Materials. *MRS Bull.* **2009**, *34*, 814−821.
(53) Lee, S.; Cheng, C.; Guo, H.; Hippalgaonkar, K.; Wang, K.; Suh, J.; Liu, K.; Wu, J. Axially Engineered Metal−Insulator Phase Transition by Graded Doping VO_2 Nanowires. *J. Am. Chem. Soc.* **2013**, *135*, 4850−4855.
(54) Maeng, J.; Kim, T.-W.; Jo, G.; Lee, T. Fabrication, Structural and Electrical Characterization of VO_2 Nanowires. *Mater. Res. Bull.* **2008**, *43*, 1649−1656.
(55) Taguchi, Y.; Matsumoto, T.; Tokura, Y.; Sr, T. Dielectric Breakdown of One-Dimensional Mott Insulators Sr_2CuO_3 and $SrCuO_2$. *Phys. Rev. B* **2000**, *62*, 7015−7018.
(56) Maki, K. Thermal Fluctuations of the Order Parameter in Charge-Density Waves. *Phys. Rev. B* **1986**, *33*, 2852−2854.
(57) Sharoni, A.; Ramírez, J.; Schuller, I. Multiple Avalanches across the Metal-Insulator Transition of Vanadium Oxide Nanoscaled Junctions. *Phys. Rev. Lett.* **2008**, *101*, 026404.
(58) Stabile, A. A.; Singh, S. K.; Wu, T.; Banerjee, S.; Sambandamurthy, G. Separating Electric Field and Thermal Effects across the Metal-Insulator Transition in Vanadium Oxide Nanobeams. *arXiv.org, e-Print Arch., Condens. Matter* **2014**, arXiv:1401.4129v1 [cond-mat.str-el].